Journal of the Chinese Chemical Society, 1999, 46, 409-416

Molecular Vibronic Structures of HDITC in Solutions Studied by Femtosecond Wavelength-Resolved Pump-Probe Spectroscopy

T.-S. Yang*[a] (楊子萱), P. Vöhringer[b], W. Dietz[c],
N. F. Scherer[d] and S. H. Lin[a,e] (林聖賢)
[a]*Institute of Atomic and Molecular Sciences, Academia Sinica, Taipei 106, R.O.C.*
[b]*Max-Planck-Institut für Biophysikalische Chemie, Am Faßberg, D-37077 Göttingen, Germany, and Universität Karlsruhe, Institut für Physik. Chemie, Kaiserstr. 12, D-76128 Karlsruhe, Germany*
[c]*Institut für Theoretische physik, Physik Department der Technischen Universität Muenchen, James-Franck-Strasse, 85747, Garching, Germany*
[d]*Department of Chemistry, the James Franck Institute and the Institute for Biophysical Dynamics, University of Chicago, Chicago, IL 60637, U.S.A.*
[e]*Department of Chemistry and Biochemistry, Arizona State University, Tempe, AZ 85287-1604, U.S.A.*

Wavelength-resolved pump-probe measurements using 11 fs duration pulses were performed to study the vibronic structures of HDITC, a cyanine dye, in ethylene glycol. Ten vibrational modes were observed in the forms of quantum beats. The frequencies of these ten vibrational modes ranged from 135 cm^{-1} to 1300 cm^{-1}. The relative potential displacements along these ten vibrational coordinates were estimated by comparison with theoretical calculations.

INTRODUCTION

The knowledge of molecular vibronic potential surfaces is essential for the study of molecular dynamics. The information on detailed molecular vibronic structures, however, is difficult to obtain in condensed media where the system-bath interactions obscure the vibronic transitions. Resonance Raman scattering is a conventional tool to obtain vibronic structures in condensed media, but it has limitations too. In the case of the molecules having a strong fluorescence with a little redshift, Raman signals are overwhelmed by the fluorescence. In 1986, Tang's group first observed quantum beats of large dye molecules in solutions, using the femtosecond transmission correlation technique.[1] They showed that the quantum beats were due to interference between coherently excited vibrational levels,[2-4] and therefore the beat frequencies were commensurate with the energy spacings between the vibrational levels. Their pioneer work implied the possibility of using the spectral width of the short pulse to resolve the molecular vibrational frequencies. Pollard et al. further applied the wave packet theory to describe the spectral evolution of quantum beats.[5,6] In the wave packet picture, the pump beam generates nonstationary wave packets in the electronic excited state as well as the ground state. The evolutions of these wave packets are governed by the vibronic Hamiltonians of the system. Subsequently the probe beam interrogates the nonstationary wave packets at delay time τ. The 3D plot of the intensity of quantum beats as a function of probe time delay and probe wavelength components reflects the temporal and spatial propagations of the wave packets on the potential surfaces. By the spectral analysis of the time-resolved pump-probe spectra, one can in turn know the potential surfaces where the wave packets propagate. These results heralded a new way of using time domain techniques to obtain frequency domain information.

In the present study, we applied the aforementioned idea to study the relative geometry of the potential surfaces of 1,1′,3,3,3′,3′-hexamethyl-4,4′,5,5′-dibenzo-2,2′-indotricarbocyanine (HDITC), a cyanine dye, in ethylene glycol solution. This molecule and a similar dye HITC have previously been used in the study of ultrafast dynamics in solutions[7-12] because their absorptions fall within the wavelength region of the Ti:sapphire laser. Information about the vibronic structures of these molecules is, however, very limited since these dye molecules exhibit very strong fluorescence in the concerned energy range. We performed wavelength-resolved pump-probe (WRPP) measurements on this molecule with 11 fs duration pump and probe pulses. The 11 fs pulse, centered at 799 nm, had a spectral FWHM of 86 nm. This allowed us to observe the vibrational frequencies up to 1400 cm^{-1}. Ten oscillatory frequencies in the range of 30 cm^{-1} to 1400 cm^{-1} were observed. The experimental results were compared with the theoretical calculations to obtain the potential surface information.

EXPERIMENTAL

The laser system used for obtaining 11 fs pulses has been described in great detail elsewhere.[13,8] Briefly, a home-built Kerr lens mode locked Ti:sapphire laser pumped by a 5W CW argon ion laser yielded a train of pulses centered at 800 nm with a repetition rate of 85 MHz and ~15 fs autocorrelation time. The pulse power spectrum had a FWHM of 86 nm (see Fig. 1).

The sample of HDITC dye (Exciton) in ethylene glycol was pumped through a nozzle, forming a jet with a thickness of 100 μm. The optical density of the jet at 780 nm was maintained at 0.3 or less. The pump energy at the sample was 1-2 nJ and probe energy was 10 to 20 times lower than that. After passing through the sample, the probe beam was dispersed in a spectrometer. The intensity of the selected wavelength component was detected by a photomultiplier (Hamamatsu R928) and the signal was processed by a lock-in amplifier (SRS-850).

ANALYTICAL METHOD

In a pump-probe measurement, the system is subjected to two pulses, viz. the pump pulse and the time-delayed probe pulse. One detects the difference in the absorption of the probe beam in the presence and in the absence of the pump beam. We considered the material polarization expanded in the Taylor series of the electric field under a weak field limit. In an isotropic medium, the total integrated difference probe intensity, $S(\tau)$, written in the lowest order is[14,15]

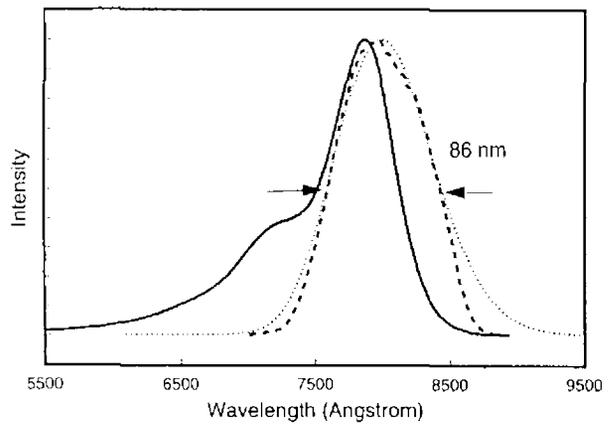

Fig. 1. The absorption spectrum of HDITC/EG and the laser power spectra. Solid line: experimental absorption spectrum; dashed line: experimental power spectrum of the laser pulses; dotted line: model power spectrum of the laser pulses.

$$S(\tau) = -2\mathrm{Im}\int_{-\infty}^{\infty} dt\ E_2^*(t-\tau)P_{k_2}^{(3)}(t,\tau) \tag{1}$$

where τ is the time delay of the probe pulse relative to the pump pulse; $E_2^*(t-\tau)$ denotes the conjugated temporal envelope of the probe field; and $P_{k_2}^{(3)}(t,\tau)$ represents the material third order polarization with wave vector k_2.

The difference probe intensity is the integration of differential probe intensity $S'(\omega,\tau)$, which has nontrivial values over the probe spectral width. We then have

$$S(\tau) \equiv \int_{-\infty}^{\infty} d\omega\ S'(\omega,\tau) \tag{2}$$

The differential probe intensity $S'(\omega,\tau)$ can be obtained by dispersing the difference probe intensity $S(\tau)$ through a monochromator and detecting the signal at frequency ω with spectral resolution $d\omega$. Writing the components of the integral in Eq. 1 in term of their Fourier components and comparing with Eq. 2, we obtain[14]

$$S'(\omega,\tau) = -2\mathrm{Im}\hat{E}_2^*(\omega)\hat{P}_{k_2}^{(3)}(\omega,\tau) \tag{3}$$

The system under investigation consists of two electronic states separated by electronic 0-0 energy ω_{eg}. The system Hamiltonian in the Born-Oppenheimer approximation can be separated into electronic and nuclear parts. The electronic broadening function can further be partitioned into inhomogeneous and homogeneous contributions. The inhomogeneous broadening is treated in this study by integrating a distribution, $G(\omega_{eg})$, around the mean value ω_c, while the homogeneous broadening function is represented as $H(t)$. In case of the pump pulse and probe pulse being temporally well separated, the material third order polarization can be written as[6,14]

$$\begin{aligned}
P^{(3)}(t,\tau) = i^3 \int_{-\infty}^{\infty} dt_3 \int_{-\infty}^{\infty} dt_2 \int_{-\infty}^{\infty} dt_1 \mathcal{H}(t_3)\mathcal{H}(t_1) \\
\times\{(R_1(t_3,t_2,t_1) + R_4(t_3,t_2,t_1)) \\
\times e^{-i(\omega_c-\Omega_2)t_3}e^{-i(\omega_c-\Omega_1)t_1} \times \mathcal{G}(t_3+t_1) \\
\times E_2(t-t_3-\tau)E_1^*(t-t_3-t_2) \\
\times E_1(t-t_3-t_2-t_1) \\
+(R_2(t_3,t_2,t_1) + R_3(t_3,t_2,t_1)) \\
\times e^{-i(\omega_c-\Omega_2)t_3}e^{i(\omega_c-\Omega_1)t_1} \times \mathcal{G}(t_3-t_1) \\
\times E_2(t-t_3-\tau)E_1(t-t_3-t_2) \\
\times E_1^*(t-t_3-t_2-t_1)\}
\end{aligned} \tag{4}$$

where

$$G(t) = \int_{-\infty}^{\infty} d\omega_{eg}\, \mathcal{G}(\omega_{eg}) e^{-i(\omega_{eg}-\omega_c)t} \quad (5)$$

The material nuclear response functions $R_n(t_3, t_2, t_1)$ expressed in terms of the lineshape function $g(t)$ are given as[16]

$$\begin{aligned} R_1(t_3,t_2,t_1) &= \exp\{-g^*(t_3) - g(t_1) - f_+(t_1+t_2+t_3)\} \\ R_2(t_3,t_2,t_1) &= \exp\{-g^*(t_3) - g^*(t_1) + f_+^*(t_1+t_2+t_3)\} \\ R_3(t_3,t_2,t_1) &= \exp\{-g(t_3) - g^*(t_1) + f_-^*(t_1+t_2+t_3)\} \\ R_4(t_3,t_2,t_1) &= \exp\{-g(t_3) - g(t_1) - f_-(t_1+t_2+t_3)\} \end{aligned} \quad (6)$$

where

$$\begin{aligned} f_+(t_1+t_2+t_3) &= g^*(t_2) - g^*(t_2+t_3) \\ &\quad -g(t_1+t_2) + g(t_1+t_2+t_3) \\ f_-(t_1+t_2+t_3) &= g(t_2) - g(t_2+t_3) \\ &\quad -g(t_1+t_2) + g(t_1+t_2+t_3) \end{aligned} \quad (7)$$

$g(t)$ counts the contributions from a variety of nuclear dynamics. For molecules undergoing frictionless harmonic oscillations with finite coherence times $1/\gamma_i$, the lineshape function takes the form as

$$\begin{aligned} g_h(t) = \sum_i S_i[&(\langle n_i\rangle + 1)(e^{-i\omega_i t - \gamma_i t} - 1) \\ &+ \langle n_i\rangle (e^{i\omega_i t - \gamma_i t} - 1)], \end{aligned} \quad (8)$$

where $S_i = \Delta_i^2/2$ and $\langle n_i\rangle = 1/(e^{\hbar\omega_i/k_BT} - 1)$. Here S_i denotes the Huang-Rhys factor, Δ_i is the dimensionless displacement of the equilibrium position between the excited state and the ground state potential surface along the dimensionless vibrational coordinate x_i, and $\langle n_i\rangle$ is the thermal occupation number of the ith vibrational mode.

Under similar approximations, the linear absorption and fluorescence cross sections can be calculated by

$$\begin{aligned} \sigma_A(\omega) &\propto \omega \times \int_0^{\infty} dt \exp[i(\omega-\omega_0)t]\exp[-g(t)] \\ \sigma_F(\omega) &\propto \omega^3 \times \int_0^{\infty} dt \exp[i(\omega-\omega_0)t]\exp[-g^*(t)]. \end{aligned} \quad (9)$$

EXPERIMENTAL RESULTS AND NUMERICAL ANALYSIS

Fig. 1 shows the overlay of the absorption spectrum of HDITC dye in ethylene glycol with the experimental and model laser pulse power spectra. The experimental power spectrum is as recorded on the spectrometer equipped with a photomultiplier (Hamamatsu R928) without further intensity calibration. The model pulse power spectrum was used in the calculations of the pump-probe signals. It has a Gaussian form centered at 799 nm with the pulse duration FWHM of 11 fs.

Fig. 2 shows the wavelength-resolved pump-probe spectra in the range of 705 nm to 855 nm. Each signal contains a small oscillatory component above the large offset. All the signals have been scaled to match the offsets in the picosecond time region so that the ratios of the oscillatory amplitudes relative to the offsets can be compared. As is clearly seen the oscillatory frequencies as well as the ratios of the oscillatory amplitudes to the offsets are higher at both ends of the probe wavelength components than at the center. The ratios at the red side of the probe spectrum are even higher than those at the blue side. These phenomena are

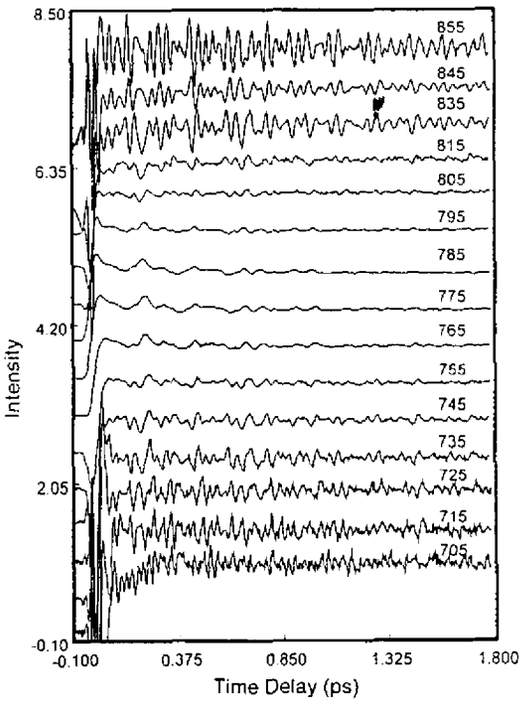

Fig. 2. Experimental wavelength-resolved pump-probe signals of HDITC/EG obtained with 11 fs duration pulses.

consistent with the prediction of the wave packet picture developed by Pollard et al.[6] They pointed out that the strongest oscillation was expected to be at a wavelength where the slope of the linear absorption is greatest, while the weakest modulation would be expected around the maximum of the linear spectrum where the slope is zero. The offsets can be fitted by two exponential functions with a fast time constant of about 200 fs and a slow time constant of about a few tens of picoseconds.

Fig. 3 displays the Fourier power spectra of the oscillatory components in Fig. 2. The oscillatory component of each WRPP spectrum was obtained prior to the Fourier transformation by subtraction of the offset using two exponential functions. Each Fourier power spectrum was plotted in the region of 30 cm^{-1} to 1400 cm^{-1} and was normalized with respect to the highest peak in this region. The spectral width of the laser pulse allowed observing vibrational frequencies up to 1400 cm^{-1}. Any peak intensities below 30 cm^{-1} are not reliable since the WRPP signals were only recorded up to 1.8 ps. Hence, the features appearing below 30 cm^{-1} are probably due to insufficient subtraction of the offset. In the wavelength range of 765 to 795 nm, the spectra are dominated by the 135 and 296 cm^{-1} peaks. The high frequency modes become prevalent toward the red as well as blue sides of the pulse wavelength components. We can

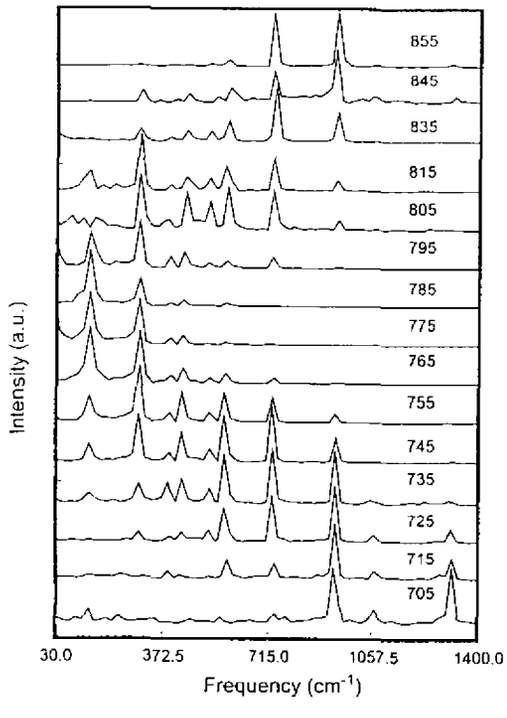

Fig. 3. Fourier power spectra of the experimental 11 fs pulse wavelength-resolved pump-probe signals of HDITC/EG.

visualize the PP signals as being the results of wave packets moving on the electronic excited state or/and on the ground state potential surfaces.[5,6] The transition wavelengths of the wave packet at boundaries of the potential surfaces set the extremes of the wavelength region where the vibrational coherence (i.e. oscillatory component) can be observed. These extremes are determined by the vibrational frequency and the relative potential displacement along the vibrational coordinate. Since the potential surface along the vibrational coordinate of a higher frequency mode has a steeper curvature, the oscillations can be observed in a wider spectral range. Also, for a vibrational mode, the larger the relative displacement is, the wider the spectral range can oscillations be observed. The study of wavelength dependence of the oscillatory amplitudes in WRPP spectra enabled us to obtain the relative potential displacements along the vibrational coordinates.

In addition to Fourier transformation, the amplitudes, frequencies, absolute phase angles, and decay rates of the oscillatory components were also analyzed using the linear prediction singular value decomposition with the assumption that the experimental data can be represented by a sum of exponentially damped cosinusoidal functions:

$$S_{pp}(\tau) = \sum_i A_i \cos(\omega_i \tau + \phi_i) \exp(-\gamma_i \tau) \qquad (10)$$

The wavelength-averaged frequencies and decay time constants of the 10 resolved vibrational coherences, thus obtained, are listed in Table 1.

The frequency of a vibrational quantum beat corresponds to the energy spacing between two vibrational levels. After examining the various possible assignments for these 10 resolved frequencies, these were assigned as the fundamental vibrational frequencies of the chromophore (see the discussion section). The relative displacements of the electronic potential surfaces along the 10 corresponding vibrational coordinates and electronic parameters were estimated by fitting the wavelength-resolved pump-probe spectra and the absorption spectrum. The four-fold integration for $P^{(3)}(\omega, \tau)$, including the three-fold integrals of Eq. 4 plus Fourier transformation of $P^{(3)}(t, \tau)$ over t, were calculated using a Monte Carlo integration routine.[17] The precision was set at 1%. The electronic homogeneous broadening function was assumed to be a simple exponential decay function $e^{-\gamma t}$ while the inhomogeneous broadening took a Gaussian distribution. Including 0-0 energy, γ_e, an inhomogeneous width, and the 10 vibrational displacements, i.e. total 13 parameters, were fitted to the absorption spectrum and 13 wavelength-resolved pump-probe spectra in the range of

Table 1. Parameters of the 10 Resolved Vibrational Modes in Wavelength-resolved Pump-probe Spectra of HDITC in Ethylene Glycol

$\omega(cm^{-1})$	135	297	396	436	526	575	730	936	1057	1310
$\gamma(cm^{-1})$	12	8	6	5	5	6	4	5	6	8
ratios of Δ	1	0.55	0.3	0.3	0.25	0.3	0.27	0.27	0.18	0.23

ω is the vibrational frequency, γ is the averaged vibrational dephasing rate, and Δ is the unitless potential displacement.

725 nm to 855 nm. The calculated intensities of the spectra of 705 nm and 715 nm were too small to afford good converged results and were hence not used.

In the fitting process, we found that the present WRPP spectra could only determine the relative magnitudes of the displacements along the 10 vibrational coordinates. This is because we did not know the absolute intensity of each WRPP spectrum. Therefore the Stokes shift was used to set the boundaries for displacements. The experimentally measured Stokes shift is the frequency separation between the absorption and emission maxima. Results of the calculation of linear spectra suggested that the Stokes shift was dominated by the displacement of the 135 cm^{-1} mode. The displacements of all other modes were small compared to that of 135 cm^{-1} mode, which broadened the linear spectra but did not shift the positions of the maxima. Therefore the experimental Stokes shift of 480 cm^{-1} sets the upper limit of $\Delta = 1.9$ for the displacement of the 135 cm^{-1} mode. We further found that if the displacement of 135 cm^{-1} mode was larger than 1, the displacements of the higher frequency modes determined relative to it through the WRPP spectra would be too big so that the intensity on the blue side of absorption maximum would be overestimated. The displacement of 135 cm^{-1} mode should hence be less than 1. When we gradually reduced the displacement of the 135 cm^{-1} mode below 1, the ratio of the oscillation amplitude vs. the offset in the WRPP spectra decreased and approached the experimental value but, on the other hand, the calculated shoulder intensities of the linear spectra decreased and deviated from the experimental data. Although the vibrational modes with frequencies higher than 1400 cm^{-1} could contribute to the shoulder intensity, their contributions would be mainly on the blue side of the shoulder because of their higher frequencies. The red side of the absorption shoulder should be dominated by the modes with frequencies less than 1400 cm^{-1}. As a compromise to these two opposite tendencies, we calculated the case that the displacement of the 135 cm^{-1} mode was set to be 0.6. The ratios of displacements of all other modes determined relative to it are listed in Table 1.

Fig. 4 shows the Fourier power spectra of the calculated pump-probe spectra using the aforementioned vibrational parameters. The electronic parameters were determined by fitting the absorption spectra as 12620 cm^{-1} for 0-0 energy, 20 cm^{-1} for the electronic dephasing rate γ_e, and FWHM of 753 cm^{-1} for the inhomogeneous width. Each spectrum in Fig. 4 is normalized by the highest peak. It can be seen that the calculated spectra reproduce the general features of the spectra in Fig. 3. The low frequency modes show strong intensities around the center wavelength components and the high frequency modes show the dominating effect on both sides.

The most obvious difference between the calculated

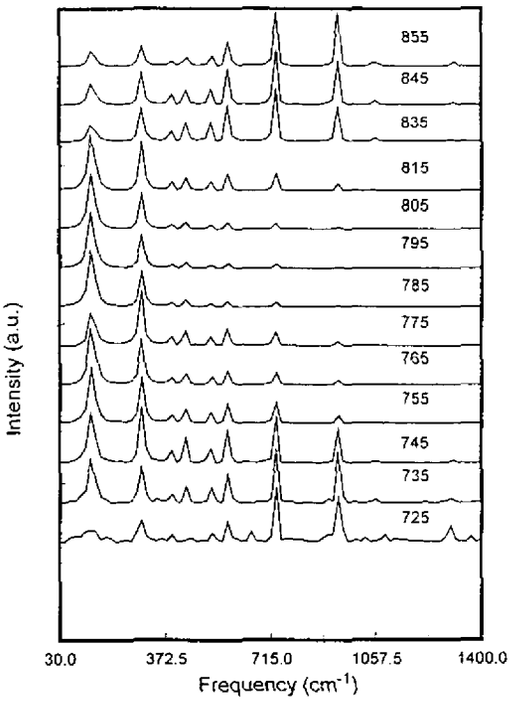

Fig. 4. Fourier power spectra of the calculated 11 fs pulse duration wavelength-resolved pump-probe signals of HDITC/EG. The dimensionless potential displacements for the 10 vibrational mdoes are 0.6 (135 cm^{-1}), 0.33 (297 cm^{-1}), 0.18 (396 cm^{-1}), 0.18 (436 cm^{-1}), 0.15 (526 cm^{-1}), 0.18 (575 cm^{-1}), 0.16 (730 cm^{-1}), 0.16 (936 cm^{-1}), 0.11 (1057 cm^{-1}), and 0.14 (1310 cm^{-1}). See text for the electronic parameters.

and experimental WRPP spectra is that the calculated intensities of the low frequency modes of 135 cm^{-1} and 296 cm^{-1} decrease more slowly on both sides of the probe wavelength components than the experimental ones. In the real system, low frequency modes usually exhibit anharmonicity and/or mode couplings to other vibrational degrees of freedom. A wave packet is the superposition of multiple vibrational states. The blue wavelength components of the probe beam induce transitions between the high energy vibrational states of the electronic excited state and bottom states of the electronic ground state while the red wavelengths induce transitions between the high energy states of the electronic ground state and the low energy states of the electronic excited state. The density of states increase with potential energy. The mode coupling became more effective with the increase of the density of states. In addition, the energies of the vibrational modes with frequencies less than or close to the thermal energy k_BT can be easily transferred to other modes through thermally induced energy matches. Therefore, the effects of mode couplings should be strong on high vibrational states of the low frequency modes which interact with both sides of the probe wavelengths. Meanwhile, anharmonicity becomes more obvious at high vibrational levels. The difference between the model and real pulse power spectra might also be responsible for the deviation.

Fig. 5 shows the 3D plots of the calculated WRPP spectra viewed from both sides of the probe wavelength components. In comparison to the absorption spectrum, the spectral shape at each delay time was limited by the pulse spectral width. The strongest intensity occurs only around maximum absorption because the potential displacements along the vibrational coordinates are all very small and therefore the centers of the wave packets move only within a few manometers. The motions of the wave packets can still be clearly visualized through the curves cut perpendicularly to the wavelength axis. At 220 fs, which is about one vibrational cycle of the 135 cm^{-1} mode, the probe intensity shows a peak on the blue side of the probe wavelengths and a valley on the red side, while at 370 fs, the three second of the vibrational cycle, the peak occurs on the red side of the probe wavelengths and the valley on the blue side. These phenomena correspond to the wave packet moving from one turning point of the potential surface to the other turning point.

DISCUSSION

11 fs pump-probe measurements resolved 10 oscillatory frequencies ranged from 30 cm^{-1} to 1400 cm^{-1}. Among them, the three lowest frequencies of 135 cm^{-1}, 297 cm^{-1}, and 396 cm^{-1} were resolved for the first time for this type of cyanine dye molecule. While the strong pump scattering interferes with the Raman scattering measurements on the low vibrational frequencies, the pump-probe measurement using a ultrashort pulse is particularly useful to study the low vibrational frequencies covered within the laser spectral width.

The 11 fs wavelength-resolved pump-probe measurements also allow us to study the relative geometries of potential surfaces in the optical resonance for this type of dye for the first time. There were only postresonant Raman scattering data available[18] before because these dye molecules exhibit the strong fluorescence with little red shift.

We have assumed earlier in the data analysis that the 10 resolved oscillatory frequencies in the WRPP spectra are the fundamental vibrational frequencies for both the electronic excited as well as ground states. This assumption is based on the conclusions drawn by examining the other pos-

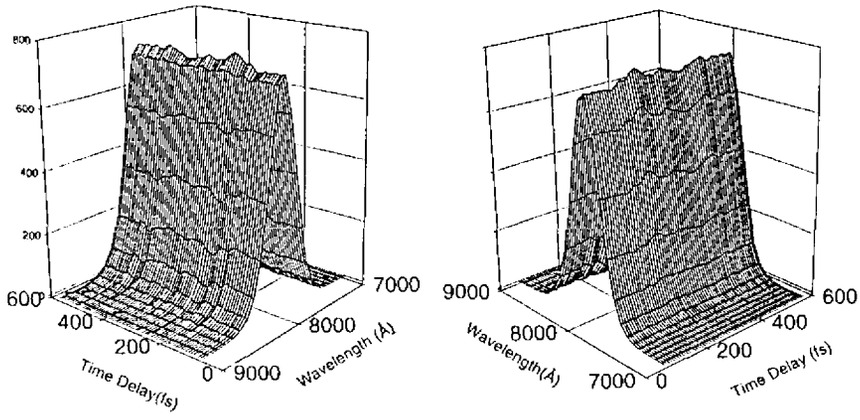

Fig. 5. 3D plots of the calculated 11 fs pulse duration wavelength-resolved pump-probe spectra as a function of probe wavelength components and probe time delay.

sible assignments. For instance, 730 cm^{-1} might be the combination band of 297 cm^{-1} and 436 cm^{-1} modes. This possibility can be ruled out because the dephasing rate of 730 cm^{-1} coherence is found to be lower than those of two low frequency coherences (see Table 1). The second case is that 135 cm^{-1}, 297 cm^{-1}, 396 cm^{-1}, 526 cm^{-1} could be the progression of the 135 cm^{-1} mode. However, it is noted that the oscillation of the first overtone frequency can be observed only when the displacement of the 135 cm^{-1} mode is larger than 1. This condition is contradictory to the requirement for fitting the absorption spectrum (see the discussion in the result section). In contrast, the assignment of small displacements for all vibrational modes happens to be self-consistent, with the assurance that overtones cannot be observed and all the frequencies are fundamental frequencies. The other ambiguity is that any two resolved frequencies might originate from a distorted vibrational mode upon excitation. Since the geometry and the dipole moment of the molecule did not change significantly upon the excitation, it is expected that modes with vibrational frequencies larger than 700 cm^{-1} will not be distorted. Several combinations of two low frequencies ($\leq$ 600 cm^{-1}) for a distorted vibrational mode do not yield the spectral feature exhibited in Fig. 2, i.e. the relative intensities of lower frequency coherences compared to those of the high frequency coherences decrease from the center to the sides of the probe wavelength components. The calculation with the assumption that all frequencies are fundamental frequencies only yields the best fit to the experimental data.

The deviation of the calculated intensities of 135 cm^{-1} modes in the WRPP spectra from the experimental data at both ends of the probe wavelength components indicates that a simple harmonic oscillator is not adequate to describe the motion associated with this mode. This deviation could be due to the anharmonicity and/or mode couplings in the real system. Nevertheless, it demonstrates that the WRPP signals are sensitive to the detailed structures of the potential surfaces and dynamics, providing more information than we could model by far.

We have calculated the relative ratios of the potential displacements along the ten vibrational coordinates. The determination of absolute values of the potential displacements needs more experimental data and theoretical analysis and is in progress.

CONCLUSION

We report here observation of rich oscillatory structures in 11 fs wavelength-resolved pump-probe signals. The Fourier transform and analysis of singular value decomposition of the oscillatory components resolved ten frequencies. Among them, the three lowest frequencies of 135 cm^{-1}, 297 cm^{-1}, and 396 cm^{-1} are resolved for the first time for this type of cyanine dye molecule. All ten frequencies are assigned as fundamental vibrational frequencies of both electronic excited and ground states. The relative potential displacements of the ten vibrational modes are obtained by fitting the absorption spectrum and the relative intensities of oscillatory components of the 13 wavelength-resolved pump-probe spectra using the molecular third order polarization. The results show that all displacements are smaller than 1. The lowest two vibrational modes of 135 cm^{-1} and 297 cm^{-1} exhibit the largest displacements while the highest two vibrational modes of 1057 cm^{-1} and 1310 cm^{-1} exhibit the smallest displacements.

ACKNOWLEDGMENT

TSY thanks Dr. R. Chang and Dr. M. Hayashi for valuable discussions and the Academia Sinica for a postdoctoral fellowship.

Received August 3, 1998.

Key Words

Femtosecond; Wavelength-resolved pump-probe; Vibronic structure.

REFERENCES

1. Rosker, M. J.; Wise, F. W.; Tang, C. L. *Phys. Rev. Lett.* **1986**, *57*, 321.
2. Mitsunaga, M.; Tang, C. L. *Phys. Rev. A* **1987**, *35*, 1720.
3. Walmsley, I. A.; Mitsunaga, M.; Tang, C. L. *Phys. Rev. A* **1988**, *38*, 4681.
4. Walmsley, I. A.; Wise, F. W.; Tang, C. L. *Chem. Phys. Lett.* **1989**, *154*, 315.
5. Pollard, W. T.; Lee, S.-Y.; Mathies, R. A. *J. Chem. Phys.* **1990**, *92*, 4012.
6. Pollard, W. T.; Dexheimer, S. L.; Wang, Q.; Peteanu, L. A.; Shank, C. V.; Mathies, R. A. *J. Phys. Chem.* **1992**, *96*, 6147.
7. Vöhringer, P.; Arnett, D. C.; Westervelt, R. A.; Feldstein, M. J.; Scherer, N. F. *J. Chem. Phys.* **1995**, *102*, 4027.
8. Vöhringer, P.; Westervelt, R. A.; Yang, T.-S.; Arnett, D. C.; Feldstein, M. J.; Scherer, N. F. *J. Raman Spectrosc.*

1995, *26*, 535.
9. Vöhringer, P.; Arnett, D. C.; Yang, T.-S.; Scherer, N. F. *Chem. Phys. Lett.* **1995**, *237*, 387.
10. Cong, P.; Yan, Y. J.; Deuel, H. P.; Simon, J. D. *J. Chem. Phys.* **1994**, *100*, 7855.
11. Martini, I.; Hartland, G. V. *Chem. Phys. Lett.* **1996**, *258*, 180.
12. Martini, I.; Hartland, G. V. *J. Phys. Chem.* **1996**, *100*, 19764.
13. Vöhringer, P.; Scherer, N. F. *J. Phys. Chem.* **1995**, *99*, 2684.
14. Yan, Y. J.; Mukamel, S. *Phys. Rev. A* **1990**, *41*, 6485.
15. Yan, Y. J.; Fried, L. E.; Mukamel, S. *J. Phys. Chem.* **1989**, *93*, 8149.
16. Yan, Y. J.; Mukamel, S. *J. Chem. Phys.* **1988**, *89*, 5160.
17. Press, W. H.; Teukolsky, S. A.; Vetterling, W. T.; Flannery, B. P. *Numerical Recipes*. Cambridge University press, New York, 2nd ed., **1992**.
18. Sato, H.; Kawasaki, M.; Kasatani, K.; Katsumata, M. *J. Raman Spectrosc.* **1988**, *19*, 129.